Materials & Design 241 (2024) 112880

Contents lists available at ScienceDirect

Materials & Design

journal homepage: www.elsevier.com/locate/matdes

Size effects in fatigue crack growth in confined volumes: A microbending case study on nanocrystalline nickel

Jutta Luksch [a,*], Aloshious Lambai [b], Gaurav Mohanty [b], Christoph Pauly [c], Florian Schaefer [a], Christian Motz [a]

[a] Materials Science and Methods, Saarland University, Saarbruecken, 66123, Germany
[b] Materials Science and Environmental Engineering, Tampere University, Tampere, 33014, Finland
[c] Chair of Functional Materials, Saarland University, Saarbruecken, 66123, Germany

ARTICLE INFO

Keywords:
Fatigue crack growth
Micro cantilever
In-situ testing
Focused ion beam

ABSTRACT

Mechanical size effects are a well known phenomenon when the sample volume is reduced or the characteristic length of the microstructure is changed. While size effects in micropillar compression (smaller is stronger) or due to grain refinement (Hall-Petch) are well understood, this is less so in fracture mechanics. Given this lack of knowledge, the main question addressed in this work is: What happens to the fatigue crack growth properties when extrinsic size effects play a role? To answer this question, nanocrystalline nickel cantilevers, ranging in width from 5 to 50 μm, were subjected to fatigue crack growth. The crack growth rates and stress intensity factors were calculated and the Paris exponent in the stable crack growth regime was determined. It was found that the results scatter more strongly for the smaller cantilevers compared to the larger cantilevers. Results are interpreted in terms of plastic zone size and ligament size which are found to be critical for small cantilevers.

1. Introduction

Materials testing of micro- and nano-scaled specimens has found its way into materials characterisation, especially into fracture mechanics, in recent years [1,2]. These testing techniques, first established for thin film testing [3–6] and later extended to cantilevers, provide defined stress states, especially in target-prepared specimens [7–12]. Actually, the evolution of crack closure effects in the field of micro- and nano-fracture mechanics has not been investigated in detail up to now which is within the scope of the current study.

The effect of smaller volumes tested is not just a interesting question in fundamental science itself but becomes also important when components are getting smaller, as in electronics [13], micro-electro-mechanical systems (MEMS) or medical devices as stents [14,15] and implantable pressure sensors [16]. Size effects that strengthen materials and components can be considered as extrinsic (smaller is stronger, geometric) [17–19] and intrinsic size effects (material effects, microstructure) [20,21]. In fracture mechanics, size effects can emerge due to both intrinsic and extrinsic reasons. External constraints like the sample geometry or complex loading conditions are crucial and may limit the size and influence the shape of an evolving plastic zone at the crack tip (extrinsic effect) [22,23]. This is especially true for micron-sized specimens where the notch geometry and sharpness varies for different focused ion beam (FIB) operators and notch depths, in contrast to a fatigue pre-cracked specimen.

For example, a change in the density of internal interfaces such as grain boundaries (intrinsic effect) may cause an increase in strength and a transition in deformation mechanisms and, therefore, the fracture behaviour and toughness. Whenever the critical length scale of the material or sample, whether grain size or sample dimensions reaches the order of magnitude of dislocation networks and structures, a size effect inevitably forms [24,25]. This results in a deformation dependent change in fracture behaviour, from plastic in Si to brittle failure in Pt cantilevers, when the sample size is reduced [26,27].

Size effects in quasi-static material behaviour have been studied and modelled extensively in the past decades [28–30]; size effects in fracture mechanics and material fatigue, on the other hand, have been studied significantly less. This is due to the complex test procedure, but also due to the fact that test standards and their limits do not easily permit the transfer of established testing techniques to the micro-scale.

* Corresponding author.
E-mail addresses: j.luksch@matsci.uni-saarland.de (J. Luksch), aloshious.lambai@tuni.fi (A. Lambai), gaurav.mohanty@tuni.fi (G. Mohanty), c.pauly@mx.uni-saarland.de (C. Pauly), f.schaefer@matsci.uni-sb.de (F. Schaefer), motz@matsci.uni-sb.de (C. Motz).

https://doi.org/10.1016/j.matdes.2024.112880
Received 23 January 2024; Received in revised form 7 March 2024; Accepted 22 March 2024
Available online 28 March 2024

Size effects are an intrinsic problem in fracture mechanics, even at the macroscopic scale, leading to specimen size requirements defined in various test-standards (ASTM E647 [31], ASTM E 1820 [32]). This even applies to linear elastic fracture mechanics (LEFM) and brittle materials (ASTM E 399 [33]), where in the case of a crack in a thin plate, the crack driving force does not depend on the crack length anymore but on the specimen thickness.

In 2004, Takashima and Higo [34] were the first to determine crack growth rates on FIB-prepared notched microbending cantilevers using a compliance method. They also carried out fracture mechanics experiments on cracked specimens. This method has been refined over the last years [11,35–37]. Eisenhut et al. showed that steep stress gradients caused dislocation pile-up at the neutral axis [29] and this in turn retarded fatigue crack growth [35]. Gruenewald et al. were able to show that in ductile materials, reliable fracture mechanical parameters can only be obtained in pre-cracked fatigue specimens and that J_{1C} for micro specimens is orders of magnitude lower than that for macro specimens, since a fully developed plastic zone can no longer be formed [23].

For defined stress conditions, specimens fabricated by FIB with a defined cross section and focusing on a crack growing are required. However, previous experiments have all been in the range of ligament lengths < 10 µm due to limitations in specimen fabrication in Ga FIB [11,38]. Luksch et al. successfully demonstrated fatigue crack growth in meso-scaled specimens with ligament lengths up to 50 µm by using Xe-Plasma-FIB and compared the results with those from macro specimens [39].

The aim of the present study is to investigate the fatigue crack growth in specimens of different sizes between 5 and 50 µm cantilever width made from nanocrystalline nickel (nc Ni). The optimised test protocol from [39] is again used here. Compared to most micro fracture and fatigue tests where the crack growth is analysed from a FIB milled notch, the present method applies a two-step process inspired by macro fatigue test standards. The first step is to induce a pre-crack from the FIB milled notch, and the second step is to analyse the crack growth behaviour.

The focus of this work is on the stable crack growth (Paris behaviour) obtained from the second part of the crack growth experiment. Furthermore, the crack contour and the microstructure at the crack flanks were investigated and compared for the different cantilever sizes. Finally, the underlying size effect is discussed.

2. Method

Pulsed electrodeposition (PED) was used to produce nc Ni as described in [40]. 1 g/L saccharin and 0.02 g/L 1,4-butynediol were used as additives for grain refinement. The material exhibits a mean grain size of about 30 nm (measured by X-ray diffraction (XRD)). Thus, the specimen volumes investigated here are always significantly larger than the mean grain size, so that the material can be considered homogeneous [41–43].

Wedges were made from the deposited material by standard metallographic techniques with polishing down to 1 µm (Fig. 1). All cantilever specimens have dimensions of thickness B: width W: lever arm L of 1:1:4 (Fig. 1), the crack growth in the direction of the width and in the following the cantilevers are named according to their width. For each cantilever size a minimum of three specimens were tested. Cantilever specimens of 20 µm and 50 µm width were produced using a Xenon Plasma FIB (Xe PFIB, Thermo Fisher Helios PFIB G4 CXe). Smaller cantilevers of 5 µm and 10 µm width were produced using a combination of Gallium FIB (Ga FIB, FEI Helios NanoLab600) and Xe PFIB to ensure high surface quality of the cantilevers of different sizes. Detailed parameters for FIB milling are given in Table 1.

All notches were made with Xe PFIB to keep the notch root and the crack initiation similar for all cantilever sizes investigated here. This avoids unnecessary Ga contamination of the notch root. An AS-

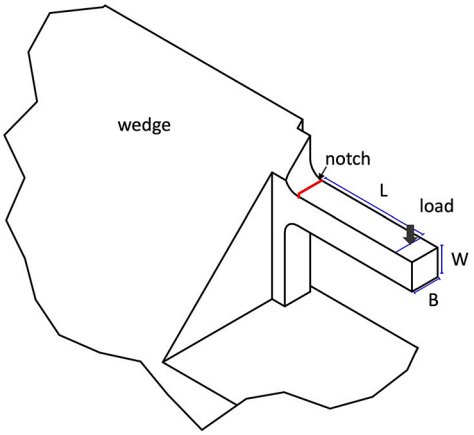

Fig. 1. Sketch of wedge with cantilever with variables of geometrical dimensions, width W, thickness B, lever arm L with ratio of B:W:L of 1:1:4.

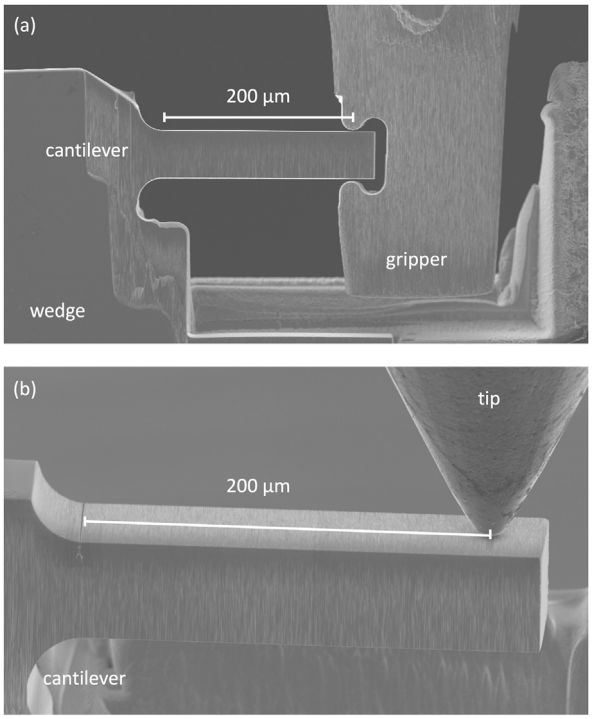

Fig. 2. SEM images from (a) crack initiation with gripper and (b) crack growth with conospherical tip.

MEC UNAT-2 with a force range from -30 to 200 mN and an ALEMNIS nanoindenter (Alemnis Standard Assembly) with a load cell from -2000 to 2000 mN be used for the *in-situ* micromechanical test in scanning electron microscopes (SEMs) (LEO and Sigma, Zeiss).

For the crack initiation that is necessary as described in [39], the theoretical flexural stress was adjusted for the cantilevers of different sizes so that a crack occurred within a few ten thousand cycles. The R ratio, $\sigma_{min}/\sigma_{max}$, was chosen between -0.2 and -0.3 for all cantilevers. To apply the negative R, as nanoindentation tip a FIB manufactured microgripper was used (Fig. 2 (a)). Crack growth is typically identified by decreasing stiffness as the stiffness can be assumed as proportional to the remaining cross section of the cantilever [44]. Since the present experiments were displacement controlled with fixed displacement amplitude, the incipient crack was identified from decreasing force amplitude.

Table 1
FIB milling and tomography parameters for the different cantilever sizes.

Cantilever	Cantilever milling parameters			Tomography milling parameters		
width	fine milling current		notch milling current	milling current		slice thickness
/ µm	/ nA	FIB	/ pA Xe	/ nA	FIB	/ nm
5	0.46	Ga	10	0.3	Ga	25
10	0.92	Ga	30	1	Xe	50
20	15	Xe	30	6.5	Ga	50
50	60	Xe	300	15	Xe	200

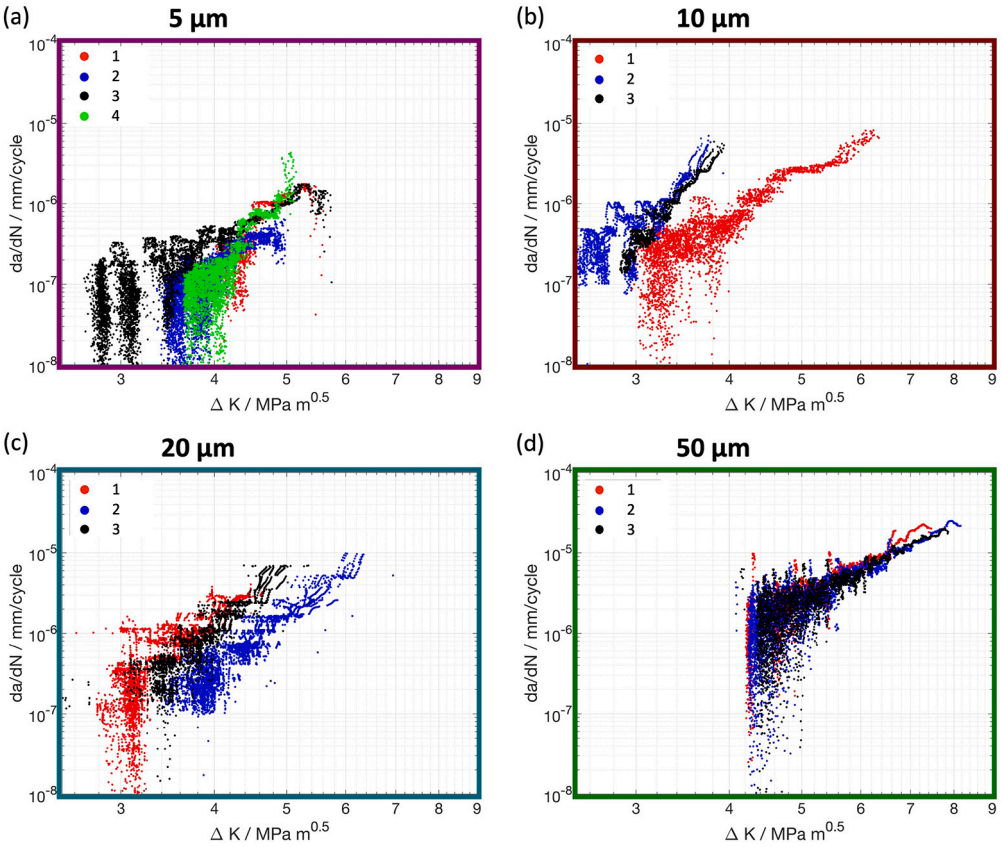

Fig. 3. Crack growth rate da/dN vs. the range of the stress intensity factor ΔK, filtered data, for the different cantilever sizes from (a) 5 µm to (d) 50 µm. All cantilevers form a linear Paris regime after the crack initiation phase.

After the crack initiation, the pre-crack length was measured in the SEM on the front and back side of the cantilevers. This was followed by the fatigue crack growth tests, which were performed with a stress ratio R of 0.1 under displacement control with force targets. Either a conospherical or a wedge tip was used in this stage (Fig. 2 (b)). The force targets were chosen with respect to the displacement applied in the crack initiation process. The loading and unloading speeds were chosen to obtain fatigue frequency of ~1 Hz.

After the da/dN test, the crack length was measured again from the front and back side on the cantilevers using SEM. The data evaluation, performed with a MATLAB® (The MathWorks Inc.) script, is described in more detail in [39]. The unloading stiffness and force amplitude for each cycle were extracted from the recorded data first. The stiffness is used to calculate the corresponding crack length under consideration of pre-crack and final crack length. Derivation yields the growth rate in each cycle. The stress intensity factor ΔK is calculated from the force amplitude per cycle, the corresponding crack length obtained from the unloading stiffness and a geometry function [45]. A moving mean filter for noise reduction was applied to the data where the frame length was adapted with respect to the number of data points. The exponent m, from the Paris-Erdogan equation, was taken from a power law fit in the Paris regime. The fit range was divided into 100 equidistant sections and the average of each section was used in the power law fit for m.

For the post-mortem analysis of the shape of a crack contour, one characteristic specimen out of each specimen size class was selected and 3D FIB serial sectioning was performed, partly with rocking polishing [46] in order to reduce curtaining at the crack tip. The parameters used are shown in Table 1. One of the 5 µm cantilevers was investigated using 3D EBSD to study microstructural changes on the crack flanks. The 3D EBSD measurement was performed using the Xe PFIB equipped with a fast CMOS EBSD camera (EDAX Velocity Plus) at 20 kV acceleration voltage and 26 nA beam current. Camera binning was set to 4x4 at exposure time of 1.7 ms, resulting in 588 fps. A step size of 25 nm on a square grid was set to match the FIB slice-to-slice thickness of the serial sectioning process. The latter was performed at 30 kV acceleration voltage and beam current of 0.3 nA. The 3D microstructure was reconstructed using the software Dream3D [47] and visualised in ParaView [48]. A data cleanup using confidence index thresholding

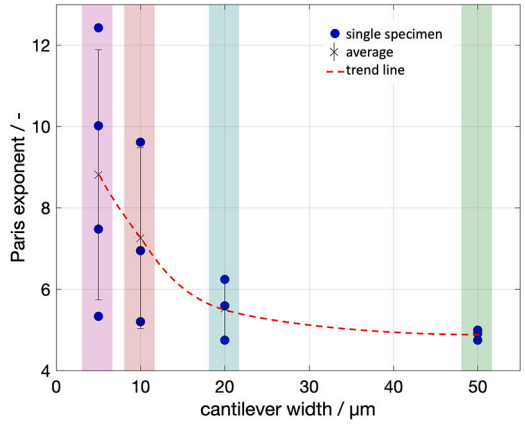

Fig. 4. Diagram of the evaluated Paris exponents with mean and error bar for each cantilever size.

(CI > 0.1) and grain dilation was part of the Dream3D reconstruction pipeline. The full reconstruction pipeline is available as supplementary material.

3. Experimental results

3.1. Crack growth rate

The crack growth rate da/dN vs. the stress intensity factor ΔK for different cantilever sizes is shown in Fig. 3. All specimens show the transition to a linear regime after the crack initiation phase. It can be clearly seen that the da/dN curves of the smaller specimens show higher scatter compared to the larger ones. This is a strong indication of an evolving extrinsic size effect.

The Paris exponent m is plotted for all tests in Fig. 4. The higher scatter of the smaller specimens is clearly reflected, too. For the larger specimens, the data collection range for crack length is significantly larger. Thus, the determined values of m are more stable and the scatter is smaller.

3.2. Crack contour

The crack contour, defined as the crack length over the cantilever thickness according [39], of one cantilever of each size was additionally investigated using 3D FIB tomography and is presented in Fig. 5.

To evaluate and compare the crack contours of the different cantilever sizes, two characteristics are considered: the curvature across the beam thickness and the scatter in the middle region of the crack contour. The crack contour for all sizes is slightly curved towards shorter crack lengths at the cantilever surface. Only the first 5 µm cantilever (Fig. 5 (a)) shows an inhomogeneity overlapping the curvature on the right side of the crack contour. The scatter of crack lengths in the middle region (insets in the diagrams of Fig. 5) is similar for all cantilevers.

3.3. Microstructure

Since extrusions were observed on the crack flanks at $R < 0$ during the crack initiation phase, a 5 µm cantilever was subjected to 3D EBSD, see Fig. 6. The EBSD analysis revealed grain coarsening in the vicinity of the crack. During the crack initiation phase, the load was applied from both sides with an R of -0.2 to -0.3, so the material was subjected to alternating tensile and compressive stress. A larger number of cycles were also applied during this $R < 0$ phase because crack initiation was not immediate and crack growth was even slower after initiation. In the crack initiation regime, grains reach a size of up to 500 nm equivalent diameter, whereas in the crack growth region, grains of up to 200 nm diameter were found. Grain orientations on both sides of the crack were observed to be identical for a number of large grains which indicates transgranular crack growth (see Fig. 6 (b) inset second row, second column).

In order to get a clear view of the interplay between crack growth rate (e.g. load history) and grain-coarsening, a cantilever with 50 µm width from previous own work [39] was analysed, too. This cantilever was subjected to a step-wise load decrease to measure ΔK_{th} according to ASTM E647 [31]. Here, each load step was applied for a few 10 000 cycles to check if the crack is still growing. The test was finished when da/dN was below 10^{-8} $^{\mathrm{mm}}/_{\mathrm{cycle}}$. That leads to ten times more cycles applied during a small crack elongation compared to the constant load phase during the crack growth rate measurement.

The cantilever was subjected to serial sectioning tomography in Xenon FIB and eight equidistant EBSD maps were recorded during sectioning. The grain size along the crack path was determined by averaging over the eight maps. Fig. 7 shows one EBSD image as example together with the depth-averaged grain size and overview of applied cycles.

It is obvious that grain growth is more pronounced in the phase of slower crack growth towards the end of the crack. This is in good agreement with the EBSD results obtained from the 5 µm cantilever mentioned above.

4. Discussion

4.1. Crack growth rate

The Paris exponent was determined for cantilevers from 5 to 50 µm using a method based on macroscopic fatigue fracture mechanics, respectively ASTM E 647 [31]. The scatter increases with decreasing cantilever width.

First a short classification of Paris exponent in macro-scale bulk metal samples is discussed. For metals, the Paris exponent in general is in the range between 2 and 5 (Al, Ni Alloys or Steel [49–51]. The here analysed nc Ni has a Paris exponent of 3 in macro-scale tests [39], so less than the in micro specimens determined Paris exponent, which was attributed to crack closure effects and the size effect.

In the current study attention should be paid to the possible sources of scattering and their different effect, depending on the specimen size. This includes the testing equipment (force resolution and control accuracy), data evaluation (crack length calculation) and the experimental procedure (indenter positioning accuracy, i.e. lever arm length). The accuracy of the force measurement (load resolution) is in the range of 4 µN, which is well below the force values applied during the test. The testing protocol requires crack length determination before and after the da/dN measurement. The crack length inside the cantilever, as obtained from the tomographies, is consistently longer than what is measured on the front and back surface. This is a well-known behaviour during fracture mechanical testing arising from a difference in the stress state between cantilever bulk and surface. There is no significant difference in the average crack lengths measured from the surface and those measured from the contour analysis after they are normalised to the cantilever widths. This suggests that the Paris exponents determined from different cantilever sizes are not systematically affected by our crack length measurements. Special attention was paid to accurately position the indenter tip to minimise the error in the lever arm length and, thus, in the stiffness calculation.

In addition to the crack contour, evaluation of the SEM images from tomographies has revealed a different appearance of the crack tip shape and flanks for the different cantilever widths, as can be seen from the SEM images in Fig. 5. The crack tip of the 5 µm specimen is more open and the crack tip is blunter. This is an indication of a higher amount of plasticity in front of the crack tip and, hence, blunting of the crack tip. The smallest specimens are at or below the lower limit of the testing standards for obtaining a valid fatigue crack growth analysis for the specific material parameters. The roughness of the crack tip contour

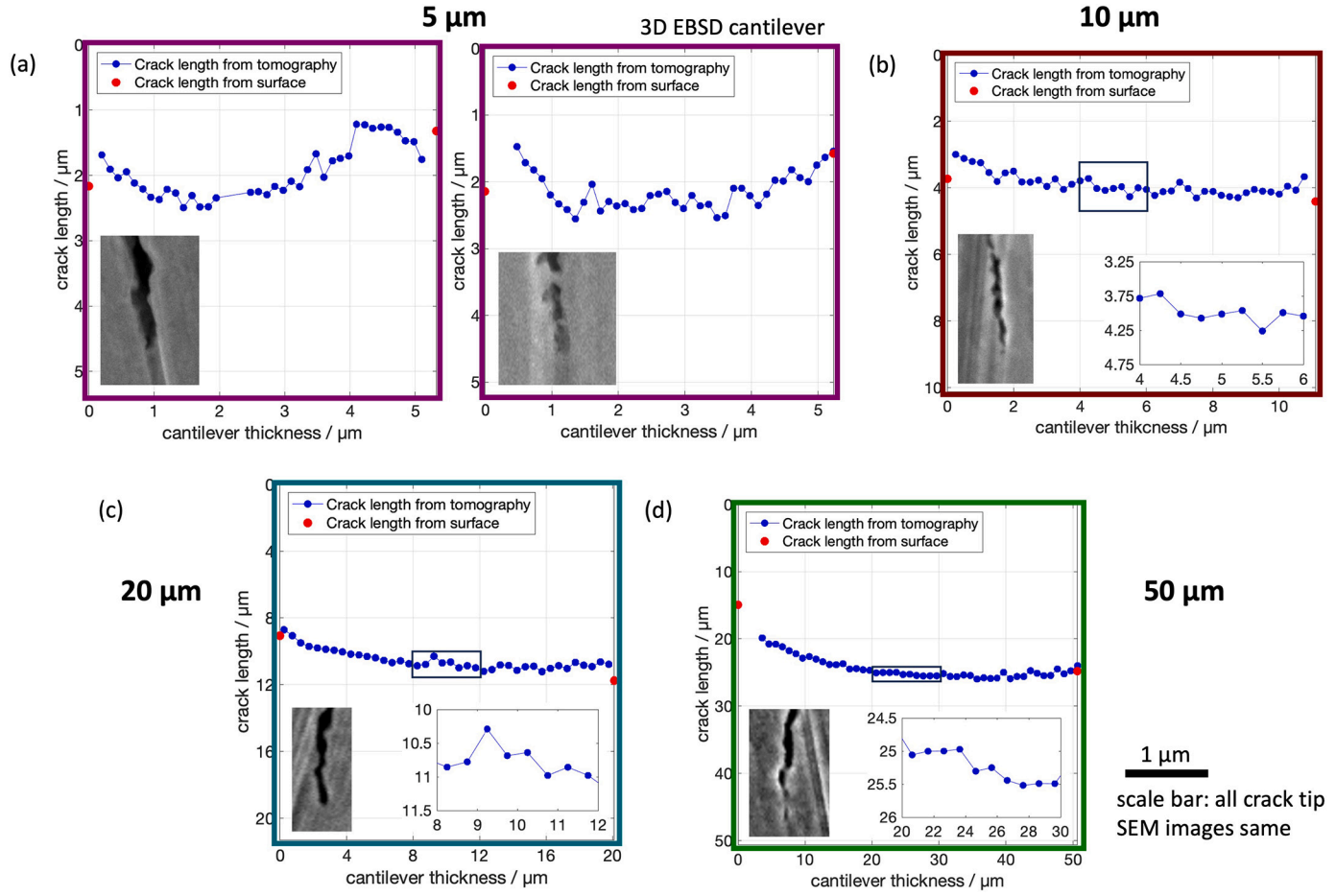

Fig. 5. Diagrams of the crack contour, assessed by 3D FIB tomography, for the different cantilever sizes from (a) 5 µm to (d) 50 µm. The inset in the diagrams of the larger cantilevers is the same scale as the 5 µm cantilever in vertical direction for better comparison of the roughness between the sizes. Additionally see the SEM images, slice from tomography in side view, from crack tip for the different cantilevers.

appears comparable for all sizes (see insets in Fig. 5 (b)-(d)). For pixel heights of 12 to 60 nm, and an approximate accuracy for manual crack length measurement of 3 pixels, the error is less than the variation in crack length.

It is obvious that the Paris regime of stable crack growth, i.e. the transition from the crack growth threshold to critical crack growth is smaller or might even vanish in the small specimens. This raises the question of whether the smaller specimens have a pronounced region of stable crack growth, and, thus, whether the determination of the Paris exponent is valid or not. In the case of a direct transition from the crack growth threshold to critical crack growth, the Paris exponent is overestimated, which is the direction of deviation in this study compared to the large cantilevers. Fig. 4 reveals that m not only scatters but its average also shifts to larger values with decreasing specimen size. This appears to be related to a larger scattering in da/dN determination when specimen size decreases as discussed above. Hence, it can be concluded that m increases when the specimen size decreases.

4.2. Microstructure

It is known that fatigue can induce grain growth especially in nc materials [52]. This adiffusional, mechanically-driven process depends on the stability of the microstructure. Kapp et al. revealed grain growth in ultra-fine grained copper to be driven by accumulated plastic strain, rather than by stress, using cyclic micro-fatigue experiments [53].

In the special case of fatigue crack growth, grain growth can take place during crack initiation and crack growth phase [54] or even before that [55]. Due to the high stress and strain, grain growth in most cases takes place in front of the crack in its plastic zone. Boyce et al. [56] found that grain growth is more pronounced in the crack initiation region than in the later crack growth in bending fatigue of nc Ni and nc Ni alloys. This may be due to larger number of cycles and, thus, a large accumulated plastic strain in the initiation region than in the later crack growth region, with a higher crack growth rate. Therefore, grain growth in the crack vicinity must be taken into account for every crack growth investigation in materials that are susceptible to microstructural instability. It is important to be aware of microstructural changes and always to characterise grain growth in addition to crack growth.

The 3D EBSD tomography of the 5 µm specimen in Fig. 6, demonstrates that large number of cycles to initiate a crack from a notch must be avoided as this can cause grains to grow, while the coarsening in the Paris exponent extraction regime is less pronounced. The transgranular nature of the crack growth in the initiation region reveals a crack growth in front of the notch.

As grain size affects the crack growth rate, larger grains from prior grain growth have a stronger impact for smaller ligament lengths in the smaller specimens, especially in the 5 µm cantilevers. This might be the origin of scatter there, as discussed above in Sec. 4.1.

Furthermore, when determining crack growth thresholds, special attention must be paid to grain growth as several 10 000 cycles are applied in a very small crack length range. The same holds true when the crack stops and thus the grains grow very large (see Fig. 7). All these effects can also appear in macro testing, but the change in microstructure relative to the specimen size is less compared to the micro specimens.

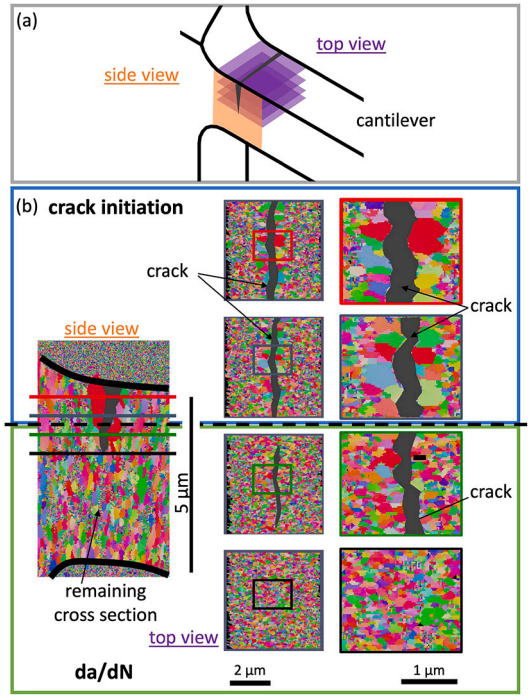

Fig. 6. (a) Sketch of a cantilever with the top and side view marked, (b) EBSD image of the tomography of 5 µm width cantilever, showing different grain sizes in the crack initiation part (blue box) and the part where the crack growth rate, da/dN, (green box) was measured for Paris exponent calculation.

4.3. Fracture mechanics

Testing protocol

Experimental challenges in meso- and microscale testing arise from fact that it is not possible to simply shrink macro-scale specimens and testing equipment. With decreasing dimensions, the accuracy of force and displacement measurement decreases, the challenge of exact sample alignment and indenter positioning increases, giving rise to systematic errors. For a more detailed consideration, the reader is referred to our previous study [39].

Size effects

As described in Section 1, size effects are typically separated into intrinsic and extrinsic. Intrinsic size effects originate from material characteristics such as defects or grain boundaries, e.g. the Hall-Petch effect. In the present study, an intrinsic size effect due to the nc microstructure is present but identical for all cantilevers and, therefore, is not considered further. Extrinsic size effects originate from the fact that the specimen size decreases independent of the aforementioned characteristic length scales of the material itself. In our case, sources for an extrinsic size effect are the plastic zone size and the ligament size. Using Irwin's model (Eq. (1)), the size of the plastic zone can be estimated from the yield stress σ_y and the stress intensity factor K_I

$$r_{pl} = \frac{1}{2\pi} \times \left(\frac{K_I}{\sigma_Y} \right)^2, \tag{1}$$

σ_y can be taken from macroscopic tensile tests. Here, the offset yield stress $R_{p0.2}$ instead of σ_y was used because of the continuous transition from elastic to plastic deformation. Using an $R_{p0.2}$ of 1070 MPa and the maximum applied K_{max} values for the respective cantilevers, a range of plastic zone sizes was calculated. For the largest cantilever, a maximum K_{max} of 10 MPa$\sqrt{\text{m}}$ results in an estimated plastic zone size of 13.9 µm while in case of the smallest cantilever, a maximum K_{max} of 5.5 MPa$\sqrt{\text{m}}$ gives an estimated plastic zone size of 4.2 µm. Comparing these values with the ligament sizes, it is clear that for the largest cantilever the ligament size is about twice the size of the plastic zone, whereas for the smallest cantilever the ligament size is about the same size or even smaller than the plastic zone, raising the question of whether LEFM is still applicable for the smallest cantilevers. This can lead to a rapid transition from crack initiation to unstable crack growth in small cantilevers or an arising plastic collapse during fracture caused by a cross-talk of blunting and back-face plasticity. This coincides with a severe reduction in the fracture toughness parameters like J_{IC}, as already discussed in the introduction.

Stress distribution

Regarding the stress distribution in cantilever bending, there exists a well-known linear stress distribution across the cantilever width with a transition from tensile to compressive stresses and the presence of a neutral axis in the centre of an unnotched cantilever (Fig. 8 (a)). Keeping the surface stress constant while reducing the cantilever width results in a steeper gradient. A more detailed evaluation of the evolution of the plastic zone in micro-bending is given in [57]. As the crack propagates, the ligament size determines the position of the neutral axis (Fig. 8 (b)). A crack growth of Δa results in a shift of the neutral axis by $0.5 \cdot \Delta a$, i.e. the crack tip and therefore the plastic zone moves closer to the neutral axis during the experiment. This has two consequences. Firstly, the stress gradient due to bending becomes steeper over time as the maximum force during crack growth is fixed but the ligament shrinks. Secondly, the interaction of the plastic zone stress field and the bending stress gradient close to the neutral axis becomes more pronounced over time. It should be noted that the cyclic plastic zone is smaller than the quasi-static one so that the onset of an extrinsic size effect is likely to be shifted to smaller specimen dimensions. Nevertheless, an interplay of plastic zone and neutral axis can be expected in small cantilevers and is likely to affect crack propagation. For large cantilevers, it can be concluded that a crack growth experiment below the limits of established standards still provides valid da/dN curves and that a strong extrinsic size effect start to occur at a smaller cantilever size as expected from standards and Eq. (1).

5. Conclusion

A detailed investigation of fatigue crack growth size effect in cantilevers with a width from 5 µm to 50 µm has been carried out, always using the identical testing and analysis protocol. The resulting da/dN curves have been compared and the Paris exponents m reveal an onset of a size effect in fatigue crack growth below 50 µm cantilever width. FIB tomography revealed severe grain growth at the crack flanks by strain accumulation, especially in the crack initiation regime and during ΔK_{th} testing. The main outcomes of this investigation are:

- Fatigue pre-crack ensures consistent da/dN curves in the investigated cantilevers from 5 µm to 50 µm.
- For sample sizes smaller than 10 µm, reproducible and valid crack growth curves can be determined using the method presented here. This is possible as long as intrinsic size effects from the material itself can be neglected, even if the scatter increases significantly towards smaller cantilevers.
- The scatter in the Paris exponent m and its average value increase with decreasing specimen size, indicating an extrinsic size effect in fatigue fracture. This extrinsic size effect was attributed to a progressively vanishing Paris regime for smaller specimens and the free surface that interacts mechanically with the plastic zone. The onset of this size effect is expected to be further shifted to smaller specimen sizes when larger stress gradients are applied in bending, compared to uniaxial testing.
- Fatigue cracks in nanocrystalline material lead to grain growth in their vicinity. In the case of slow crack growth or crack arrest as well as during the crack initiation period, very strong grain growth occurs in the vicinity of the crack tip, depending on the accumulated strain. This causes inhomogeneities in the material and,

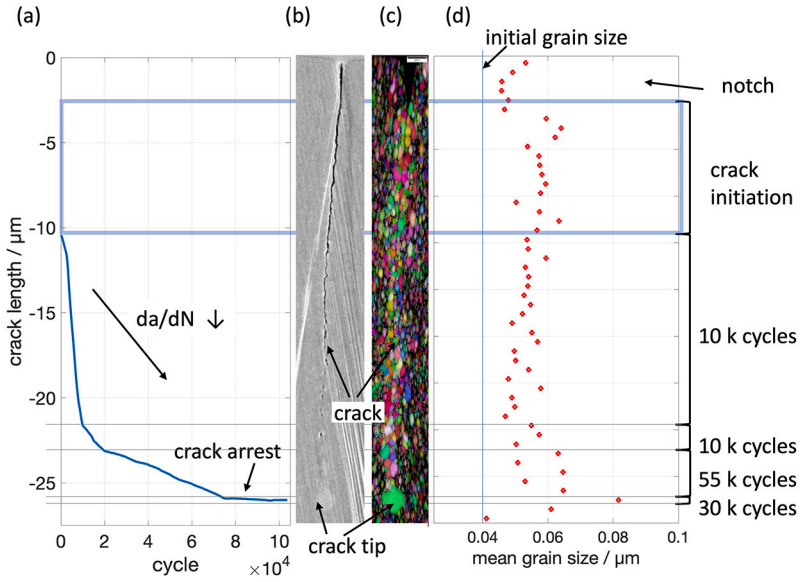

Fig. 7. Summarised data from ΔK_{th} specimen, 50 µm width. (a) crack length over applied cycles, (b) SEM image of slice 1 taken from tomography, (c) EBSD inverse pole figure and image quality map of the same slice and (d) grain size analysis along the crack. Largest grains are found where most cycles were applied.

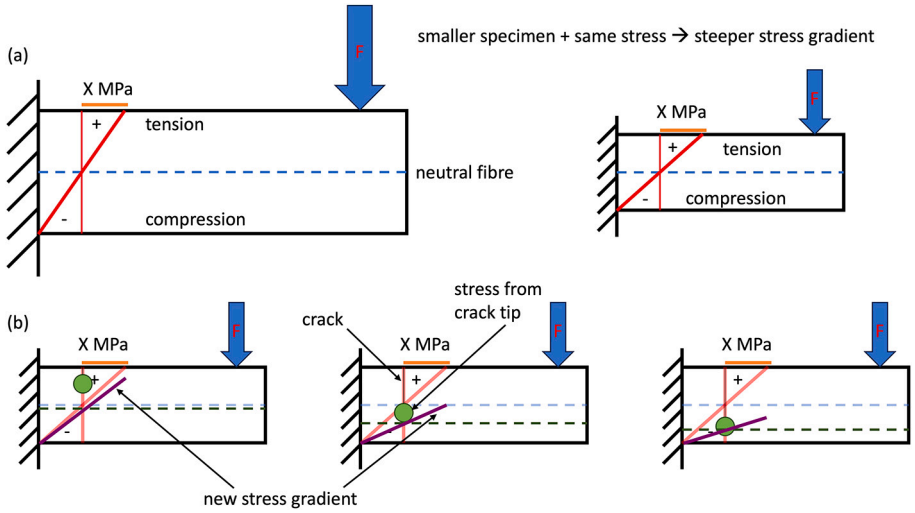

Fig. 8. (a) 2D schematic distribution of stress in cantilever bending, comparison of cantilever sizes with same maximal stress (X MPa) and influence on stress gradient in red. (b) Influence of crack length on stress gradient (new stress gradient in purpel) and overlaying with stress from crack tip, schematically shown as a green circle.

depending on their extent, must be taken into account for further evaluations.

The last point of the main outcomes can be used to investigate cyclic grain growth in more detail in future studies. Overall, the interaction between microstructure, boundary conditions and experimental testing is very complex and further specific investigations are required to fully understand the influence of grain growth on crack growth and vice versa.

CRediT authorship contribution statement

Jutta Luksch: Writing – original draft, Visualization, Validation, Methodology, Investigation, Formal analysis. **Aloshious Lambai:** Writing – review & editing, Investigation. **Gaurav Mohanty:** Writing – review & editing, Supervision, Resources, Funding acquisition. **Christoph Pauly:** Writing – review & editing, Resources, Investigation, Formal analysis. **Florian Schaefer:** Writing – review & editing, Funding acquisition, Formal analysis. **Christian Motz:** Writing – review & editing, Supervision, Resources, Funding acquisition, Conceptualization.

Declaration of competing interest

The authors declare that they have no known competing financial interests or personal relationships that could have appeared to influence the work reported in this paper.

Data availability

Data will be made available on request.

Acknowledgements

Funding by Deutsche Forschungsgemeinschaft (DFG) for project funding 521371248 and the Plasma-FIB/SEM (INST 256/510-1 FUGG) is greatly acknowledged. GM and AL acknowledge partial funding from

Academy of Finland grant number 341050. This work made use of Tampere Microscopy Center facilities at Tampere University.

Appendix A. Supplementary material

Supplementary material related to this article can be found online at https://doi.org/10.1016/j.matdes.2024.112880.

References

[1] R. Pippan, S. Wurster, D. Kiener, Fracture mechanics of micro samples: fundamental considerations, Mater. Des. 159 (2018) 252–267.

[2] D. Kiener, A. Misra, Nanomechanical characterization, Mater. Res. Soc. Bull. (2023), https://doi.org/10.1557/s43577-023-00643-z.

[3] R. Schwaiger, G. Dehm, O. Kraft, Cyclic deformation of polycrystalline cu films, Philos. Mag. 83 (6) (2003) 693–710, https://doi.org/10.1080/0141861021000056690.

[4] X.J. Sun, C.C. Wang, J. Zhang, G. Liu, G.J. Zhang, X.D. Ding, G.P. Zhang, J. Sun, Thickness dependent fatigue life at microcrack nucleation for metal thin films on flexible substrates, J. Phys. D, Appl. Phys. 41 (19) (2008) 195404, https://doi.org/10.1088/0022-3727/41/19/195404.

[5] G.-D. Sim, Y. Hwangbo, H.-H. Kim, S.-B. Lee, J.J. Vlassak, Fatigue of polymer-supported ag thin films, Scr. Mater. 66 (11) (2012) 915–918, https://doi.org/10.1016/j.scriptamat.2012.02.030, Viewpoint set no. 49: Strengthening effect of nanoscale twins.

[6] B.-J. Kim, H.-A.-S. Shin, S.-Y. Jung, Y. Cho, O. Kraft, I.-S. Choi, Y.-C. Joo, Crack nucleation during mechanical fatigue in thin metal films on flexible substrates, Acta Mater. 61 (9) (2013) 3473–3481, https://doi.org/10.1016/j.actamat.2013.02.041.

[7] D. Kupka, E.T. Lilleodden, Mechanical testing of solid–solid interfaces at the microscale, Exp. Mech. 52 (6) (2012) 649–658, https://doi.org/10.1007/s11340-011-9530-z.

[8] J. Luksch, A. Jung, C. Pauly, R. Derr, P. Gruenewald, M. Laub, M. Klaus, C. Genzel, C. Motz, F. Mücklich, F. Schaefer, Ni/al-hybrid cellular foams: an interface study by combination of 3d-phase morphology imaging, microbeam fracture mechanics and in situ synchrotron stress analysis, Materials 14 (2021), https://doi.org/10.3390/ma14133473.

[9] W. Zhang, Z. Ma, D. Liu, S. Wang, H. Zhao, L. Ren, Synergetic strengthening of coherent and incoherent interface on a mixed-phase high-entropy alloy revealed by micro-pillar compression, J. Mater. Res. Technol. 18 (2022) 3777–3784, https://doi.org/10.1016/j.jmrt.2022.04.064.

[10] S. Lavenstein, J.A. El-Awady, Micro-scale fatigue mechanisms in metals: insights gained from small-scale experiments and discrete dislocation dynamics simulations, https://doi.org/10.1016/j.cossms.2019.07.004, 2019.

[11] S. Gabel, B. Merle, E. Bitzek, M. Göken, A new method for microscale cyclic crack growth characterization from notched microcantilevers and application to single crystalline tungsten and a metallic glass, J. Mater. Res. 37 (12) (2022) 2061–2072, https://doi.org/10.1557/s43578-022-00618-x.

[12] M. Wurmshuber, M. Alfreider, S. Wurster, M. Burtscher, R. Pippan, D. Kiener, Small-scale fracture mechanical investigations on grain boundary doped ultrafine-grained tungsten, Acta Mater. 250 (2023) 118878, https://doi.org/10.1016/j.actamat.2023.118878.

[13] I. Stachiv, E. Alarcon, M. Lamac, Shape memory alloys and polymers for mems/nems applications: review on recent findings and challenges in design, preparation, and characterization, Metals 11 (3) (2021), https://doi.org/10.3390/met11030415.

[14] A.R. Pelton, B.T. Berg, P. Saffari, A.P. Stebner, A.N. Bucsek, Pre-strain and mean strain effects on the fatigue behavior of superelastic nitinol medical devices, Shape Mem. Superelast. 8 (2) (2022) 64–84, https://doi.org/10.1007/s40830-022-00377-y.

[15] J.L. Gugat, C. Bechtold, C. Chluba, E. Quandt, R.L. de Miranda, High-cycle mechanical fatigue performance of sputtered nitinol, J. Mater. Eng. Perform. 29 (3) (2020) 1892–1900, https://doi.org/10.1007/s11665-020-04668-2.

[16] N.K. Sodavaram, D. McCormick, F. Alam, J. Potgieter, D.M. Budgett, K.M. Arif, Modeling, simulation and experimental validation of fatigue behavior of thin-film titanium membranes, Microsyst. Technol. 25 (9) (2019) 3489–3501, https://doi.org/10.1007/s00542-018-4230-6.

[17] E. Arzt, Size effects in materials due to microstructural and dimensional constraints: a comparative review, Process Saf. Environ. Prot. 77 (6) (1998) 371–372, https://doi.org/10.1016/S1359-6454(98)00231-6.

[18] M.D. Uchic, D.M. Dimiduk, A methodology to investigate size scale effects in crystalline plasticity using uniaxial compression testing, Mater. Sci. Eng. A 400–401 (2005) 268–278, https://doi.org/10.1016/j.msea.2005.03.082.

[19] J.R. Greer, J.T.M. De Hosson, Plasticity in small-sized metallic systems: intrinsic versus extrinsic size effect, Prog. Mater. Sci. 56 (6) (2011) 654–724, https://doi.org/10.1016/j.pmatsci.2011.01.005.

[20] B.N. Jaya, C. Kirchlechner, G. Dehm, Can microscale fracture tests provide reliable fracture toughness values? A case study in silicon, J. Mater. Res. 30 (5) (2015) 686–698, https://doi.org/10.1557/jmr.2015.2.

[21] J.P. Wharry, K.H. Yano, P.V. Patki, Intrinsic-extrinsic size effect relationship for micromechanical tests, Scr. Mater. 162 (2019) 63–67, https://doi.org/10.1016/j.scriptamat.2018.10.045.

[22] S. Wurster, C. Motz, R. Pippan, Characterization of the fracture toughness of micro-sized tungsten single crystal notched specimens, Philos. Mag. 92 (14) (2012) 1803–1825, https://doi.org/10.1080/14786435.2012.658449.

[23] P. Gruenewald, F. Schaefer, M. Thielen, M. Marx, C. Motz, Small scale fracture mechanics of ductile materials: advantage of fatigue precracks and comparison of J-integral evaluations, Materialia 4 (2018) 104–108, https://doi.org/10.1016/j.mtla.2018.09.011.

[24] C. Trinks, C.A. Volkert, Transition from dislocation glide to creep controlled damage in fatigued thin Cu films, J. Appl. Phys. 114 (9) (2013) 093510, https://doi.org/10.1063/1.4819760, https://pubs.aip.org/aip/jap/article-pdf/doi/10.1063/1.4819760/13466634/093510_1_online.pdf.

[25] J. Rafael Velayarce, C. Motz, Effect of sample size and crystal orientation on the fatigue behaviour of single crystalline microbeams, Materials 13 (3) (2020) 741, https://doi.org/10.3390/ma13030741.

[26] B.N. Jaya, V. Jayaram, Fracture testing at small-length scales: from plasticity in si to brittleness in pt, JOM 68 (2016) 94–108, https://doi.org/10.1007/s11837-015-1489-2.

[27] I. Issa, C. Gammer, S. Kolitsch, A. Hohenwarter, P.J. Imrich, R. Pippan, D. Kiener, In-situ tem investigation of toughening in silicon at small scales, Mater. Today 48 (2021) 29–37, https://doi.org/10.1016/j.mattod.2021.03.009.

[28] N. Fleck, G. Muller, M.F. Ashby, J.W. Hutchinson, Strain gradient plasticity: theory and experiment, Acta Metall. Mater. 42 (2) (1994) 475–487, https://doi.org/10.1016/0956-7151(94)90502-9.

[29] C. Motz, T. Schöberl, R. Pippan, Mechanical properties of micro-sized copper bending beams machined by the focused ion beam technique, Acta Mater. 53 (15) (2005) 4269–4279, https://doi.org/10.1016/j.actamat.2005.05.036.

[30] F. Iqbal, J. Ast, M. Göken, K. Durst, In situ micro-cantilever tests to study fracture properties of nial single crystals, Acta Mater. 60 (3) (2012) 1193–1200, https://doi.org/10.1016/j.actamat.2011.10.060.

[31] ASTM E647-13: Standard Test Method for Measurement of Fatigue Crack Growth Rates, Standard, American Society for Testing and Materials, 2013.

[32] ASTM-E1820-11: Standard Test Method for Measurement of Fracture Toughness, Standard, American Society for Testing and Materials, 2011.

[33] ASTM-E399-123: Standard Test Method for plane-strain fracture toughness of metallic materials, in: Annual book of ASTM Standards, Standard, American Society for Testing and Materials, 2012.

[34] K. Takashima, Y. Higo, Fatigue and fracture of a Ni–P amorphous alloy thin film on the micrometer scale, Fatigue Fract. Eng. Mater. Struct. 28 (8) (2005) 703–710, https://doi.org/10.1111/j.1460-2695.2005.00923.x.

[35] L. Eisenhut, F. Schaefer, P. Gruenewald, L. Weiter, M. Marx, C. Motz, Effect of a dislocation pile-up at the neutral axis on trans-crystalline crack growth for micro-bending fatigue, Int. J. Fatigue 94 (2017) 131–139, https://doi.org/10.1016/j.ijfatigue.2016.09.015.

[36] P. Gruenewald, J. Rauber, M. Marx, C. Motz, F. Schaefer, Acquiring in situ fatigue crack growth curves by a compliance method for micro bending beams to reveal the interaction of fatigue cracks with grain boundaries, Proc. Struct. Int. 17 (2019) 13–20, https://doi.org/10.1016/j.prostr.2019.08.003.

[37] P. Gruenewald, J. Rauber, M. Marx, C. Motz, F. Schaefer, Fatigue crack growth in micro specimens as a tool to measure crack – microstructure interactions, Fatigue Fract. Eng. Mater. Struct. 43 (2020) 3037–3049, https://doi.org/10.1111/ffe.13354.

[38] J. Ast, M. Ghidelli, K. Durst, M. Göken, M. Sebastiani, A.M. Korsunsky, A review of experimental approaches to fracture toughness evaluation at the micro-scale, Mater. Des. 173 (2019) 107762, https://doi.org/10.1016/j.matdes.2019.107762.

[39] J. Luksch, A. Lambai, G. Mohanty, F. Schaefer, C. Motz, Bridging macro to micro-scale fatigue crack growth by advanced fracture mechanical testing on the meso-scale, Mater. Sci. Eng. A (2023) 145452, https://doi.org/10.1016/j.msea.2023.145452.

[40] K. Schueler, B. Philippi, M. Weinmann, V.M. Marx, H. Vehoff, Effects of processing on texture, internal stresses and mechanical properties during the pulsed electrodeposition of nanocrystalline and ultrafine-grained nickel, Acta Mater. 61 (2013) 3945–3955, https://doi.org/10.1016/j.actamat.2013.03.008.

[41] J. Wehrs, G. Mohanty, G. Guillonneau, A.A. Taylor, X. Maeder, D. Frey, L. Philippe, S. Mischler, J.M. Wheeler, J. Michler, Comparison of in situ micromechanical strain-rate sensitivity measurement techniques, JOM 67 (2015) 1684–1693, https://doi.org/10.1007/s11837-015-1447-z.

[42] V. Maier, K. Durst, J. Mueller, B. Backes, H.W. Höppel, M. Göken, Nanoindentation strain-rate jump tests for determining the local strain-rate sensitivity in nanocrystalline ni and ultrafine-grained al, J. Mater. Res. 26 (11) (2011) 1421–1430, https://doi.org/10.1557/jmr.2011.156.

[43] G. Mohanty, J. Wehrs, B.L. Boyce, A. Taylor, M. Hasegawa, L. Philippe, J. Michler, Room temperature stress relaxation in nanocrystalline ni measured by micropillar compression and miniature tension, J. Mater. Res. 31 (8) (2016) 1085–1095, https://doi.org/10.1557/jmr.2016.101.

[44] M. Alfreider, D. Kozic, O. Kolednik, D. Kiener, In-situ elastic-plastic fracture mechanics on the microscale by means of continuous dynamical testing, Mater. Des. 148 (2018) 177–187, https://doi.org/10.1016/j.matdes.2018.03.051.

[45] S. Wurster, C. Motz, R. Pippan, Notched-cantilever testing on the micrometer scale - effects of constraints on plasticity and fracture behaviour, 2010.

[46] L. Kwakman, G. Franz, M.M.V. Taklo, A. Klumpp, P. Ramm, Characterization and failure analysis of 3d integrated systems using a novel plasma-fib system, AIP Conf. Proc. 1395 (1) (2011) 269–273, https://doi.org/10.1063/1.3657902.

[47] M.A. Groeber, M.A. Jackson, Dream. 3d: a digital representation environment for the analysis of microstructure in 3d, Integr. Mater. Manuf. Innov. 3 (2014) 56–72.
[48] J. Ahrens, B. Geveci, C. Law, C. Hansen, C. Johnson, ParaView: an end-user tool for large-data visualization, in: The Visualization Handbook, 2005, pp. 717–731.
[49] S. Klysz, G. Gmurczyk, J. Lisiecki, Investigations of some properties of material samples taken from the aircraft withdrawn from service, Fatigue Aircr. Struct. 2010 (2) (2010) 52–58, https://doi.org/10.2478/v10164-010-0025-7.
[50] R. Branco, F. Antunes, J. Martins Ferreira, J. Silva, Determination of Paris law constants with a reverse engineering technique, Eng. Fail. Anal. 16 (2) (March 2009) 631–638, Papers presented at the 24th meeting of the Spanish Fracture Group (Burgos, Spain, March 2007), https://doi.org/10.1016/j.engfailanal.2008.02.004.
[51] S. Chauhan, A.K. Pawar, J. Chattopadhyay, B.K. Dutta, Determination of fatigue properties using miniaturized specimens, Trans. Indian Inst. Met. 69 (2) (2016) 609–615, https://doi.org/10.1007/s12666-015-0796-1.
[52] H.A. Padilla, B.L. Boyce, A review of fatigue behavior in nanocrystalline metals, Exp. Mech. 50 (1) (2010) 5–23, https://doi.org/10.1007/s11340-009-9301-2.
[53] M.W. Kapp, T. Kremmer, C. Motz, B. Yang, R. Pippan, Structural instabilities during cyclic loading of ultrafine-grained copper studied with micro bending experiments, Acta Mater. 125 (2017) 351–358, https://doi.org/10.1016/j.actamat.2016.11.040.
[54] T.A. Furnish, A. Mehta, D. Van Campen, D.C. Bufford, K. Hattar, B.L. Boyce, The onset and evolution of fatigue-induced abnormal grain growth in nanocrystalline Ni–Fe, J. Mater. Sci. 52 (2017) 46–59, https://doi.org/10.1007/s10853-016-0437-z.
[55] T.A. Furnish, D.C. Bufford, F. Ren, A. Mehta, K. Hattar, B.L. Boyce, Evidence that abnormal grain growth precedes fatigue crack initiation in nanocrystalline Ni-Fe, Scr. Mater. 143 (2018) 15–19, https://doi.org/10.1016/j.scriptamat.2017.08.047.
[56] B.L. Boyce, H.A. Padilla, Anomalous fatigue behavior and fatigue-induced grain growth in nanocrystalline nickel alloys, Metall. Mater. Trans. A 42 (2011) 1793–1804, https://doi.org/10.1007/s11661-011-0708-x.
[57] D. Rajpoot, P. Tandaiya, R.L. Narayan, U. Ramamurty, Size effects and failure regimes in notched micro-cantilever beam fracture, Acta Mater. 234 (2022) 118041, https://doi.org/10.1016/j.actamat.2022.118041.